Oriented Co-immobilization of Oxidase and Catalase On Tailor-made Ordered Mesoporous Silica

Juan M. Bolivar[1], Victoria Gascon[2], Carlos Marquez-Alvarez[2], Rosa M. Blanco[2], Bernd Nidetzky[1,3]

[1] Institute of Biotechnology and Biochemical Engineering, Graz University of Technology, NAWI Graz, Petersgasse 12, A-8010 Graz, Austria

[2] Molecular Sieves Group, Institute of Catalysis and Petroleum Chemistry (ICP-CSIC), Marie Curie, 2, Cantoblanco 28049, Madrid, Spain

[3] Austrian Centre of Industrial Biotechnology, Petersgasse 14, A-8010 Graz, Austria

ABSTRACT

Mesoporous silica materials are promising carriers for enzyme immobilization in heterogeneous biocatalysis applications. By tailoring their pore structural framework, these materials are designable for appropriate enzyme binding capacity and internal diffusivity. To supply O_2 efficiently to solid-supported immobilized enzymes represents a core problem of heterogeneously catalyzed oxidative biotransformations. In this study, therefore, we synthesized and compared three internally well-ordered and two amorphous silica materials as enzyme carriers, each of those with pore sizes of ≥ 10 nm, to enable the co-immobilization of D-amino-acid oxidase (93 kDa) and catalase (245 kDa). Both enzymes were fused to the silica-binding module Z_{basic2} to facilitate their selective and oriented immobilization directly from crude protein mixtures on native silica materials. Analyzing the effects of varied pore architecture and internal surface area on the performance of the immobilized bienzymatic system, we showed that a uniform pore structural framework was beneficial for enzyme loading (≥ 70 mg protein/g carrier), immobilization yield ($\geq 90\%$), surface and pore volume filling without hindered adsorption, and catalytic effectiveness ($\geq 60\%$) of the co-immobilizate. Using the best carrier LP-SBA-15, we obtained a solid oxidase-catalase preparation with an activity of 2000 µmol/(min g_material) that was recyclable and stable during oxidation of D-methionine. These results affirm a strategy of optimizing immobilized O_2-dependent enzymes via tunable internal structuring of the silica material used as carrier. They thus make a significant advance towards the molecular design of heterogeneous oxidation biocatalysts on mesoporous silica supports.

INTRODUCTION

Immobilization of enzymes onto insoluble porous supports is a key technology for biocatalytic process development.[1–3] Immobilization enables the enzyme to be reused and it also facilitates the transition from batch to continuous processing. Immobilization onto supports allows practical reactor design and operation, and it generally simplifies the downstream processing. [1,4] Extra stability due to immobilization often helps to maximize the enzyme's total turnover number. [5,6] In any immobilization, the activity of the solid catalyst preparation (mass or mol product released/mass catalyst × time used) is a key critical parameter of process suitability. Its optimization therefore constitutes a major task of the development. However, to achieve an appropriate catalyst activity (*Cat*) is often complicated, for *Cat* is the result of different factors combined. Formally, *Cat* is the product of the intrinsic specific activity of the soluble enzyme (µmol product/mg enzyme min), the enzyme amount loaded on the support (mg enzyme/mg support) and the fraction activity of the soluble enzyme remaining in the immobilizate, often also referred to as the catalytic effectiveness of the immobilized enzyme.[5,7] Enzyme loading and effectiveness factors of *Cat* are critically determined by the material properties of the carrier used, because it strongly affects the enzyme attached to the solid surface[5,8–10] as well as the interplay between reaction and diffusion in the overall biocatalytic conversion.[2,10]

Among biotransformations currently considered for industrial use, the ones catalyzed by flavoenzyme oxidases struggle with special difficulties in immobilization development[11]. Stability in the presence of the reaction co-product H_2O_2 is a problem requiring particular attention[12]. Efficient supply of O_2 into the solid catalyst is another, for diffusional restrictions, and also often results in severe decreases in *Cat* due to their immediate effects on the catalytic effectiveness factor.[13–15] Supported by new analytical techniques enabling O_2 concentrations to

be measured directly inside the solid carrier,[7,14,16] development of tailor-made support materials for effective use of immobilized oxidases becomes realistic in two important directions. First, the mass transfer within the solid phase is optimized via fine-tuning of the external geometry and the internal pore framework of the support [16]. Second, in order to destroy H_2O_2 and partly regenerate O_2 within the solid phase,[12,17,18] the oxidase is efficiently co-immobilized with catalase through pores whose geometrical features enable a true co-localisation of the two enzymes inside the support. Note: catalases are relatively big molecules with an effective mass of around 250 kDa.[19–21] A material synthesis both flexible and precise to create solid supports with optimized morphology is therefore required. Mesoporous silica is highly promising, for its morphology is broadly tunable via known synthetic procedures, and silica in general is excellently biocompatible and exploitable for practical enzyme immobilization.[22,23]

Silica materials applicable to enzyme immobilization have a broad variety of forms: ordered mesopororous silicas, silica gels, vesicular silica, fumed silica and porous glass.[22–25] Ordered mesoporous silica materials (OMSM) are of special relevance.[23,26–29] They are characterized by a regular porosity in terms of pore size and pore network arrangement.[26,30] They can be tailored to offer large specific surface area, large specific pore volume, uniform pore size distribution, and chemical and mechanical stability compatible with almost any enzyme reactor design in principle. Properties of OMSM can be fine-tuned by the synthesis conditions[31–33]: the temperature and time of the key synthesis steps (hydrolysis, condensation and hydrothermal treatment)[34–36]; the organic co-solvents, the co-surfactant and/or the organic swelling agents employed[37–41]; the addition of salts to the synthesis medium[36,42]; and the type of silica precursor used.[43]

A difficult problem of immobilization on silica is to find a proper way of fixing the enzyme on the solid surface. This usually involves a significant amount of testing, with each new enzyme requiring a fresh assessment. Different types of surface functionalization and conditions for enzyme binding and coupling to the surface are evaluated.[2,10,22,30] The concept of the silica binding module aims at enzyme immobilization on silica by design[44–46] The design principle involves genetically encoded fusion of the silica-binding module to the enzyme of interest, thus conferring the ability to adsorb to plain silica surfaces to any enzyme in principle. A highly promising silica binding module is Z_{basic2}.[45,47] Z_{basic2} is a small three-helical module that is highly positively charged and so shows strong binding to negatively charged surfaces, including silica surfaces. Enzyme chimeras harboring Z_{basic2} are efficiently immobilized on plain silica-based materials.[16,45] The immobilization is highly selective, most likely because it appears to occur in a well-defined orientation via the Z_{basic2} module. It is stable under operation, yet readily reversible.[16,45] High protein loading (> 50 mg/g carrier) is possible in principle, but this depends strongly on the material properties of the OMSM used. Unfortunately, these material properties are often not ideal, or even unsuitable, for enzyme immobilization.

Aim of this study was to combine advanced material and enzyme design for the development of a highly active and stable silica immobilizate of an oxidase-catalase pair of enzymes. Besides the co-localizing immobilization of the two enzymes, which is a problem on its own, a main difficulty of oxidase-catalase co-immobilizate development is to balance the individual enzyme activities such that the oxidase activity of the solid material is maximized. Due to the extremely high specific activity of the catalase, its activity is normally present in large excess.[48] The task thus becomes to immobilize a maximum amount of oxidase (here: D-amino acid oxidase) and to make sure that the O_2 demand of the oxidase is partly fulfilled from the catalase reaction via

effective hydrogen peroxide degradation. Variation in overall silica morphology as well as in OMSM pore structural framework was used in synthetic silica materials to explore material characteristics important for efficiency in the co-immobilization of the two enzymes. Based on detailed evaluation of catalytic performance parameters of the solid enzyme immobilizates we were able to select a recyclable heterogeneous biocatalyst, which compared with the single oxidase immobilizate, was not only 1.3-fold more active but also significantly more stable. Material properties required for high enzyme effectiveness were thus identified.

MATERIALS AND METHODS

Reagents and chemicals

1,3,5-Trimetylbenzene (TMB), m-xylene (both from Aldrich, Madrid, Spain) and 1,3,5-triisopropylbenzene (TIPB; from Alfa Aesar, Heysham, United Kingdom) were used as micelle expanders. The triblock co-polymers poly(ethylene oxide)-poly(propylene oxide)-poly(ethylene oxide) Pluronic® F127 ($PEO_{106}PPO_{70}PEO_{106}$; from Sigma, Madrid, Spain) and Pluronic® P123 ($PEO_{20}PPO_{70}PEO_{20}$; from Aldrich, Poole, United Kingdom) were used as structure-directing agents. Silica source tetraethoxysilane was from Merck, (Darmstadt, Germany). Ammonium fluoride (NH_4F) was from Alfa Aesar (Heysham, United Kingdom), potassium chloride and hydrochloric acid were from Panreac (Barcelona, Spain). Porous spherical silicate particles (PSSP)[49] were from Glantreo Limited (Cork, Ireland). All reagents and solvents were of analytical grade.

Synthesis of materials

Preparation of large pore OMSM required the use of specific conditions of synthesis. FDU-12 silica with face-centered cubic arrangement of spherical mesopores with ultra-large-pore size have been obtained using Pluronic F127 ($EO_{106}PO_{70}EO_{106}$) triblock copolymer template with the

addition of 1,3,5-trimethylbenzene (TMB) or m-xylene (XYL) as powerful swelling agents and an inorganic salt (KCl) under acidic conditions.[50–53] Also 2D hexagonal ultra-large-pore SBA-15 silica was synthesized using Pluronic P123 ($EO_{20}PO_{70}EO_{20}$) surfactant, TIPB as a swelling agent and NH_4F salt under acidic conditions.[53] To prepare SBA-15 material, which is characterized by a particularly large pore size, the use of a micelle expander such as TIPB is required. SBA-15 material was synthesized according to Cao et al.[52] with some modifications described in the Electronic Supporting Information (ESI). The final material was labelled as LP-SBA-15-TIPB-C (LP: Large-pore size; SBA-15 material; TIPB as micelle expander and calcination (C) treatment). Synthesis of mesocellular foam (MCF-TIPB-C) used the same procedure as for LP-SBA-15-TIPB-C, but was performed at 15 °C instead of 18 °C. Synthesis of extra-large mesoporous FDU-12 involved xylene as micelle expander and used the procedure of Huang et al.[51] with slight modifications described in the ESI. The resulting material was designated as LP-FDU-12-XYL-C. Another FDU-12 material was synthesized using TMB according to a slightly modified literature protocol[50,54] (for details, see the ESI) and was designated as LP-FDU-12-TMB-C. It was verified by thermogravimetric analysis (TGA) that organic compounds had been removed completely from the final materials used.

Characterization methods

Low-angle X-ray diffraction (XRD) patterns were recorded using a X'PERT Pro PANalytical diffractometer using the Cu-Kα radiation (λ = 1.5406 Å). Diffraction data were recorded in the 2θ range from 0.4° to 6° with a step size of 0.02° and an accumulation time of 20 s. Transmission electron microscopy (TEM) images were acquired with a JEOL 2100F microscope, equipped with a field emission gun and operated at 200 kV, obtaining a point resolution of 0.19 nm. The images were recorded and analyzed using Gatan Microscopy suite TMs software that

operated a Gatan CCD camera. Samples for TEM analysis were prepared by dispersing a small amount of material in acetone and sonicating in an ultrasonication water bath for 30 min. A drop of this suspension was deposited onto a carbon-coated copper grid, and then allowed to dry overnight before TEM analysis. The particle morphologies were examined by scanning electron microscopy (SEM). Images were collected using a FE-SEM FEI Nova Nanosem 230 microscope equipped with vCD detector. The samples for SEM analysis were prepared by placing material powder on double-sided graphite adhesive tape mounted on the sample holder. Nitrogen adsorption-desorption isotherms of the samples were measured at -196 ºC using a Micromeritics ASAP 2420 volumetric adsorption analyser. Samples were outgassed at 350 ºC for 16 h under high vacuum before measurement. The specific surface areas were calculated by the Brunauer-Emmett-Teller (BET) method. Pore size was determined using the Barrett-Joyner-Halenda (BJH).[55] Pore diameter distribution curves were determined from the adsorption and desorption branches of the nitrogen isotherms using the BJH method. The total pore volume was determined from the amount of nitrogen adsorbed at a relative pressure of 0.98. Thermogravimetric analyses were carried out using a Perkin-Elmer TGA 7 instrument. Samples were heated in synthetic airflow from 25 ºC to 900 ºC at a rate of 20 ºC/min.

Enzymes

D-Amino acid oxidase from *Trigonopsis variabilis* (DAAO)[45,56] and catalase (CATA) from *Bordetella pertussis*[19,48] were used. Each enzyme was obtained in a chimeric form that had the Z_{basic2} module fused at the N-terminus[47,48]. Enzymes were produced recombinantly in *E. coli* BL21 DE3 as described elsewhere[47,48]. If not mentioned otherwise, *E. coli* cell extract containing DAAO or CATA was used.

Enzyme assays

Enzyme activities were obtained from initial rate measurements. One activity unit (U) refers to 1 μmol/min of substrate consumption or product formation under the conditions used. Activity of free or immobilized DAAO was determined via measurement of the oxygen consumption rate during oxidative deamination of D-Met. A fiber-optic oxygen microoptode was used and the procedures are described elsewhere in full detail.[13] In addition, the activity of soluble DAAO was determined by measuring the H_2O_2 production using a reported peroxidase-coupled assay[47]. CATA activity was determined at 30 ºC monitoring H_2O_2 consumption at 240 nm. The reaction mix consisted of 50 mM air-saturated potassium phosphate buffer, pH 8.0, containing 10 mM H_2O_2. The cell-extract activities of Z_{basic2}_DAAO and Z_{basic2}_CATA used in this study were 2 and 5000 units (U)/mg_protein, respectively. With the aim of comparing, the specific activity of purified Z_{basic2}_DAAO was 71 U/mg_protein[47], that of Z_{basic2}_catalase was 60000 U/mg_protein.[48]

Enzyme immobilization

This was performed under conditions previously optimized to enable adsorption of Z_{basic2} enzymes on underivatized silica supports with both high efficiency and controlled orientation via the Z_{basic2} module.[45] The immobilization was performed stepwise where a maximum protein concentration of 5 g/L was used in solution. Briefly, the silica materials were exhaustively rinsed with water and then incubated under mild stirring in 50 mM potassium phosphate, pH 8.0. Cell extract was brought to pH 8.0, and NaCl (1.0 M) and Tween (0.5 %) added. Silica support (~50 mg) was then mixed with 2 mL cell extract and incubated under gentle mixing at 25 °C.

Samples (50 μL) were taken at certain times from the supernatant after spinning down the solids or from the whole solid-liquid suspension. It is common in enzyme immobilization to relate the

amount of enzyme bound to the solid support to the initial enzyme loading used, which is given in mg protein or enzyme U/g solid material. This is only to clarify that protein adsorption isotherms were not used. Enzyme activity and protein concentration in supernatant were measured in each sample. The immobilization yield (%) was calculated as $100 \times (a_0 - a)/a_0$, where a_0 is initial enzyme activity and a is enzyme activity after immobilization. DAAO-CATA coimmobilization was performed sequentially, CATA before DAAO.

The distribution of immobilized DAAO on silica particles was analyzed by a reported procedure[16] which is based on confocal laser scanning microscopy and uses the enzyme's FAD cofactor as internal fluorescence reporter group. Suspensions of the solid DAAO-CATA coimmobilizate (10 mg/mL) in 50 mM potassium phosphate buffer, pH 7.0, were used in the analysis.

Catalytic effectiveness of enzyme immobilizates

The so-called stationary effectiveness factor (η) is commonly used to evaluate immobilized enzyme preparations. It is the ratio between the actual activity of the immobilizate (E_{obs}; U/g support) and the immobilizate's activity expected from the immobilization yield (E_{bound}). To measure E_{obs}, solid immobilizate (1-5 mg) was resuspended in a final volume of 4 mL air-saturated buffer (50 mM potassium phosphate buffer, pH 8.0) in a quartz cuvette equipped with magnetic stirring and temperature control (30 ºC). Activity was then determined using the assays described above.

Evaluation of enzyme immobilizates in oxidative deamination of D-Met

Reactions consisted of 5 mL solution (50 mM D-Met; 50 mM potassium phosphate, pH 8.0) containing 0.05 mg immobilizate/mL or 0.1 U soluble enzyme/mL. Incubation was done in 15

mL tubes at room temperature (~25 °C) and an end-over-end-rotator (30 rpm) was used for mixing. O_2 availability in supernatant (~90 % air saturation at atmospheric pressure) was regularly checked with the oxygen microoptode. At certain times, a homogeneous sample was withdrawn and the concentration of 2-keto-4-(methylthio)butyric acid was determined[16]. At the end of reaction, the enzyme immobilizate was recovered by centrifugation, and it was used again for new rounds of conversion.

Enzyme spatial dimension analysis

To design pores able to accommodate the enzymes used, the approximate spatial dimensions of DAAO and CATA were needed. The functional DAAO is a homodimer (Uniprot entry: Q99042; subunit size: 356 amino acids, 39.3 kDa). CATA is a homotetramer (Uniprot entry: A0A0E8DM81; subunit size: 479 amino acids, 54.2 kDa). Closely homologous enzymes that had their crystal structure determined were used to assess the spatial dimensions: DAAO from *Rhodotorula gracilis* (Protein Data Bank entry: 1C0P, Uniprot entry: P80324) and CATA from *Pseudomonas aeruginosa* (Protein Data Bank entry: 4E37, Uniprot entry: O52762). Enzyme structures were visualized with Pymol, and the molecular dimensions of the functional DAAO dimer and CATA tetramer were calculated using the Draw_Protein_Dimensions.py script. The maximum dimension of CATA was 10 nm, that of DAAO was 7 nm.

RESULTS AND DISCUSSION

The silica material synthesis was pursued with the goal of enabling the enzymes to access the internal pore surface in a relatively unhindered fashion. Considering the size of CATA and DAAO (Scheme 1), this therefore involved the task of controlling the pore size to ~10 nm or greater. It was expected that materials made porous in such a way would allow a suitable amount

of enzymes (≥ 50 mg/g_support) to become adsorbed when a large surface area was achieved (≥ 200 m^2/g_support). Pore size, pore architecture and specific surface area are key parameters of solid material morphology. Silica materials representing a significant variation in these parameters were therefore prepared and consequent effects on the enzyme immobilization and the performance of the immobilized enzymes were evaluated.

Characterization of the silica supports used

Three silica materials involved an ordered pore internal structure (LP-SBA-15-TIPB-C, LP-FDU-12-TMB-C and LP-FDU-12-XYL-C) while two were amorphous (MCF-TIPB-C and PSSP). Preparation of the large pore OMSM required the use of specific synthesis conditions described in the Experimental Section. The materials were characterized by XRD for their structural analysis (Figure 1A and Figure S1), by SEM and TEM to evaluate the morphology and internal structure of the particles (Figure 2 and Figure S2-S6), and by nitrogen adsorption to determine the porosity and textural properties of the supports (Figure 1B, Figure S7 and Table 1). The powder XRD patterns of calcined ordered mesoporous silica materials revealed the ordered spatial arrangement of the pores (Figure 1A). The data suggested a 2D hexagonal structure for LP-SBA-15-TIPB-C with an unit-cell parameter of 14 nm.[31,52,55] LP-FDU-12-TMB-C and LP-FDU-12-XYL-C exhibited well-resolved patterns characteristic of a face-centered cubic structure (*Fm3m*).[41,43,50] The unit-cell parameter was 40 nm and 46 nm, respectively. In the case of amorphous mesoporous materials (MCF-TIPB-C and PSSP), the XRD patterns only showed a broad diffraction peak at low angle, pointing to the absence of periodical order in the pore structure (see SI, Figure S1).

Nitrogen adsorption-desorption isotherms of the calcined samples are shown in Figure 1B and pore size calculations are shown in Figure S7 and Table 1. LP-SBA-15-TIPB-C showed a very

narrow pore size distribution (cf. also Figure S7A). A pore diameter of 10 nm was estimated (Figure 2, Figure S7A). FDU-12 materials displayed cage-like mesopores whose windows entrances were narrower than the cage diameter.[57,58] Cage size distributions centered at about 31 nm for LP-FDU-12-XYL-C and 18 nm for LP-FDU-12-TMB-C. The cage entrance sizes were determined from desorption-branches as 17 nm and 9 nm, respectively (Figure S7A, Figure 2). TEM images illustrate the well-ordered mesostructures of FDU-12 and SBA-15 samples, with high-quality and large-domain regularity (Figure 2). TEM images of samples LP-FDU-12-TMB-C and LP-FDU-12-XYL-C revealed projections characteristic of face-centered cubic structure ($Fm3m$)[51]. Moreover, the images of LP-SBA-15-TIPB-C material also show well-ordered mesoporous structure with hexagonal arrangement of cylindrical pore channels can be inferred in Figure 2. The data of amorphous mesoporous materials (PSSP and MCF-TIPB-C) suggested interconnected and ink-bottle shaped pores (Figure S7A, Figure 2) with broad pore size distribution. PSSP showed its maximum around 12 nm and minimum pore openings were around 7 nm in size (Figure S7 B). Data of MCF-TIPB-C suggests pore openings in the range 5 - 30 nm (Figure S7 B). All the supports had large pore channels or cavities with pore entrance sizes suitable for the uptake of both DAAO and catalase (Scheme 1).

The external morphology of the silica materials can be observed in SEM images (Figures S2-S6) and microscopy images (Figure 3 and Figure S8). PSSP displayed an almost perfect spherical shape with a diameter of 2.8 μm. FDU-12 showed an irregular polyhedron shape with a narrow distribution in size (~4−6 μm). SBA-15 predominantly existed as rod-shape amorphous particles of ~4−5 μm width. MCF-TIPB-C material displayed amorphous polyhedron shape (~4−5 μm), somewhat agglomerated particles of about 10 μm size were however also observed.

Immobilization of Z$_{basic2}$_DAAO

The different silica materials were compared in immobilization experiments in which DAAO adsorption was evaluated in dependence of the amount of enzyme offered. When only a low amount of enzyme was present, all the materials showed similar behavior and full enzyme adsorption was observed (Figure 4A). At increased enzyme loadings (1000 U/g_support, equivalent to 15 mg protein/g_support), however, the DAAO adsorption was no longer complete for some materials and the value of E_{bound} (U adsorbed/g_support) differed substantially between the different materials. Whereas PSSP and both FDU-12 materials displayed a clear saturation behavior featuring a decrease in the immobilization yield at high loading (Figure 4A and SI Figure S9), MCF-TIPB-C and in particular LP-SBA-15-TIPB-C were able to retain a linear dependence of E_{bound} on the enzyme amount offered up to 3000 U/g_support. Using SBA-15 it was possible to immobilize up to 5000 U/g_support with a yield of 90 %. It seems plausible that the different loading capacities of the silica materials used reflected differences in accessibility of their respective pore framework to the enzyme.

Incorporation of DAAO into the solid supports was visualized with CLSM based on detection of fluorescence from the enzyme-bound FAD.[16] Figure 3 shows CLSM images recorded from supports loaded with a relatively high amount of enzyme (2000 U/g_support). At this loading, clear signs of hindered immobilization were already noted for most of the silica materials, as indicated in Figure 4A. Figure 3 reveals that FAD fluorescence had penetrated completely the different silica particles, suggesting that accessibility into the solid material was not a factor restricting the enzyme immobilization. Therefore, differences between the silica materials were likely determined by parameters of the internal morphology such as porosity and specific surface area. A large enzyme-accessible specific surface area results from a suitable compromise between porosity and specific surface area to facilitate the enzyme immobilization.

To obtain insight into the degree of surface coverage by immobilized enzyme in the different silica supports, the data in Figure 4A were normalized on the unit of available surface area and are shown in Figure 4B. The three materials (LP-FDU-12-TMB-C, LP-FDU-12-XYL-C and PSSP) exhibiting small E_{bound} and early saturation in the immobilization were also the ones with the highest surface-bound activity at low enzyme loadings (2000 U/g). Their saturation behavior probably reflects restriction in enzyme accessible surface area. Differences in entrance pore size might explain the higher surface-bound activity of LP-FDU-12-XYL-C (17 nm) as compared to PSSP (7 - 12 nm) and LP-FDU-12-TMB-C (9 nm). The two other silica materials showing high E_{bound} were quite different one from another. MCF-TIPB-C gave the lowest performance of all supports, probably because from the broad pore distribution range (5 - 30 nm) in this material a large portion of entrance pores was too small for enzyme entry. The material with uniform pore framework (LP-SBA-15-TIPB-C), by contrast, excelled not only in E_{bound} but also in surface bound activity. At the highest enzyme loadings examined, LP-SBA-15-TIPB-C was even superior to the other supports regarding protein density (14 U/m^2), immobilization yield (85%), and maximum enzyme loading (5000 U/g_support). Analyzing the immobilization data in terms of pore filling[59] (Figures S10 and S11), we noted that apparent saturation was observed in LP-FDU-12 materials and PSSP already at very low degrees of pore volume usage. Only the LP-SBA-15-TIPB-C material showed an effective use of the pore volume of the support.

Catalytic activity of solid-supported DAAO

It is quite common for immobilized enzymes that the actual activity of the solid immobilizate (E_{obs}) is not the same as, typically lower than, expected from E_{bound}. Figure 5A shows how the E_{obs} of different immobilized DAAO preparations (U/g_support) changed with increasing E_{bound}. At low enzyme loadings, all immobilizates behaved similarly and E_{obs} was a full expression of

E_{bound} (Figure 5A). When the enzyme loading was increased, E_{obs} gradually dropped below E_{bound}. The FDU-12 materials were generally lowest in E_{obs}. PSSP exhibited an almost linear dependence of E_{obs} on E_{bound}. The SBA materials offered the highest maximally achievable E_{obs} that increased from 500 U/g_support for FDU-12 to 1800 U/g_support for SBA-15. The large E_{obs} for SBA-15 seemed to reflect the also high E_{bound} achievable in this material. We also note that using SBA-15 a maximum in E_{bound} was not reached in the experiment. The stationary effectiveness factor ($\eta = E_{obs}/E_{bound}$) was used to further evaluate the DAAO immobilizates in terms of their catalytic performance.

Figure 5B shows the change in η of the different imobilizates dependent on E_{obs}. At low enzyme loadings, irrespective of the silica material used, η approached a value of unity. The parameter η comprises two different effects of the immobilization on the enzymatic reaction: one is the change, typically a decrease, in the specific activity of enzyme due to its attachment on the solid surface, and the other is mass transport into and out of the porous support. Evidence that $\eta = \sim 1$ implies that the immobilization of Z_{basic2}_DAAO on the silica supports went along with near complete retention of the enzyme's specific activity. This in turn suggested a nearly ideal function of the Z_{basic2} binding module in the immobilization, anchoring the enzyme on the silica surface in a well-defined orientation via Z_{basic2}. When however E_{bound} was increased, a gradual drop in η was observed. For an E_{bound} of 500 U/g_support, the value of η was in the range 0.2 - 0.6 for the FDU-12, SBA-15 and MCF immobilizates. The decrease in η dependent on E_{bound} was curved and appeared to level out at a low but finite value at high E_{bound}. The SBA-15 support, for instance, showed η of ~ 0.4 even at the highest E_{obs} used in the experiment. Curvature in the dependence of η on E_{bound} plausibly arises as result of a transition from reaction

control of the enzymatic rate at low E_{bound} to diffusion control at high E_{bound}, as discussed elsewhere in more detail.[15,16]

We have shown by experiment of earlier work that reaction-caused depletion of the O_2 substrate within the solid support can in fact become limiting for E_{obs} of an immobilized oxidase, most notably under conditions when the E_{bound} is high.[15,60] A useful approach to attenuate diffusional restrictions at high E_{bound} is to optimize parameters of the carrier's geometry, specifically the particle size. Behavior of the PSSP immobilizates is exemplary in this regard (Figure 5B). The spherical PSSP particles with their uniformly small diameter (2.8 μm) showed the most efficient performance. The more irregular shaped and larger sized silica materials (e.g. LP-FDU-12-XYL-C; minimum dimension: 4 - 5 μm) showed by far more pronounced decrease of η dependent on E_{obs}, as shown in Figure 5. Time-scale analysis for diffusion and enzymatic reaction supported the notion of a shift in reaction control due to increase in E_{bound} (Figure S12), with diffusion becoming chiefly rate determining for an E_{bound} of about 1000 U/g_support or higher. The importance of optimizing the carrier geometry in order to maximize η of immobilized DAAO was emphasized by comparison of the silica support SBA-15 from this study with larger carriers (dimension: $\geq$ 100 μm) used previously. Whereas η of just around 0.1 was measured with these large carriers at the low maximum of E_{obs} achievable with them (~250 U/g_support), the SBA-15 immobilizate gave a much higher η value of ~0.4 at substantially elevated E_{obs} of 1800 U/g_support. These results provide a useful basis for tailoring the properties of silica materials applied to the immobilization of O_2-dependent enzymes.

Co-immobilization of DAAO and CAT for biocatalytic use

Having in mind the application of immobilized DAAO as recyclable catalyst for repeated batchwise conversions of D-Met, we co-immobilized Z_{basic2}_DAAO and Z_{basic2}_CATA. As already mentioned, degradation of H_2O_2 by CATA had the roles of regenerating some O_2 for the oxidase reaction and attenuating oxidative inactivation of the immobilized enzymes. Based on previous studies of oxidase-CATA co-immobilization[12,61,62] we chose an E_{bound} of CATA exceeding that of DAAO by 60-fold. Considering the specific activity of CATA (60000 U/mg), this implied the need to immobilize CATA protein in the range of only 0.5 - 2 mg/g_support. Results are shown in Table 2. CATA was immobilized on all supports in ~90 % yield. The value of η was between 0.4 and 0.6 at the highest E_{bound} used (Table 2). Diffusional restriction on H_2O_2 supply into the porous supports plausibly caused the effect of lowering the η under these conditions. Table 2 also shows that prior immobilization of CATA did not affect the yield of DAAO immobilization at an E_{bound} of 2000 units/g_support. FDU materials were exceptions because the DAAO yield decreased when CAT was present.

Figure 6 compares time courses of the different DAOO-CATA co-immobilizates converting D-Met into α-keto-acid. The solid catalysts were used at 0.5 g/L and each contained 2000 U of oxidase/g_support. Reaction of the soluble enzymes applied at the equivalent volumetric loading of 1000 U of oxidase/L served as reference. Due to the relatively low catalyst concentration used, surface aeration was sufficient to keep the O_2 concentration in the liquid phase at near saturation during the reaction. In each reaction, product formation was approximately linear with time. The volumetric productivity increased in the order FDU-12 < MCF < SBA-15 < PSSP as expected from the immobilizates' η. We also determined the operational effectiveness factor ($η_{op}$) of the immobilized enzymes, which we defined as the ratio of the reaction times needed with immobilizate and free enzyme to achieve 25 % substrate conversion. Table 3 shows that $η_{op}$

varied broadly between the different coimmobilizates, with LP-SBA-15-TIPB-C giving the best performance (η_{op} = ~0.6). All immobilizates were easily separated from the liquid phase by gravity sedimentation and they could be recycled at least three times (equivalent to a total operation time of 34 h) without appreciable loss in enzyme activity, as indicated by the relatively constant values of η_{op} in Table 3. By contrast, the single oxidase immobilizate in LP-SBA-15-TIPB-C not only showed a lower η_{op} (1.3-fold) but also lost most the activity after one single use, as shown in Table 3. The LP-SBA-15-TIPB-C immobilizate clearly outperformed all other silica supports regarding enzyme activity and stability.

Heterogeneous O$_2$-dependent biocatalysis designed for efficiency: limitations and opportunities

Intensification of O$_2$-dependent reactions catalyzed by enzymes immobilized on porous supports is achieved primarily by enhancement of the solid catalyst's productivity, *Cat*. Recall that *Cat* equals E$_{bound}$ × η. Scheme 2 shows a design window applicable to the systematic optimization of *Cat* via improvements in E$_{bound}$, η or both. Possible limitations are pointed out and strategies for targeted "debottlenecking" are indicated.

The enhancement of E$_{bound}$ depends on the properties of the material used, primarily surface area and pore size, as well as on the immobilization chemistry. Immobilization of oxidases was often operated at low enzyme loading[2,63–65] to eliminate diffusional effects. The important problem of how to boost the E$_{bound}$ effectively was not given sufficient attention[66]. Macroporous materials, which due to their large pore size ($\geq$ 50 nm) provide only a limited amount of internal surface area ($\leq$ 50 m^2/g), were often used. Emerging mesoporous materials however offer substantially increased surface area at reduced pore size.[22,30] Generally, as long as the enzyme is able to diffuse through the pores, surface area determines the E$_{bound}$ loadable into the support[10,67]. A key

question therefore becomes: what is, for a given immobilization chemistry, the optimum pore framework that allows for an effective use of the surface area available to the enzyme? The current study was designed to provide relevant evidence. Use of a fully reversible, ionic adsorption-based method of immobilization ensured that the enzymes could become distributed in the solid material in a truly uniform fashion. Fast covalent immobilization, by contrast, can result in trapping of the enzymes in the outermost pore areas of the solid support, so preventing that the full surface area is utilized for binding[10,68]. We furthermore synthesized silica materials whose pores were of adequate size for the enzymes to access the internal surface area. The results show that a large E_{bound} was achievable dependent on surface area, as predicted. Ordered and uniform pore frameworks were best suited to maximize the E_{bound}.

η is determined by the interplay between biochemical and physicochemical factors of the immobilization. Choice of strategy to boost η therefore depends on the controlling mechanism. The complex problem of enzyme inactivation by the immobilization procedure used[13,15,63,64] was solved, and the consequent decrease in η prevented completely, using enzyme fusion to the silica-binding module Z_{basic2}.[56,60] However, since chemical reaction and diffusion are intrinsically coupled events in transformations catalyzed by solid enzyme immobilizates, η is not independent of E_{bound} and the dependence generally starts to show at high enzyme loadings[7,14–16]. Material properties thus become important in the effort of enhancing the degree of uncoupling of η from E_{bound}. Traditional porous materials have particle sizes of 100 µm or greater. Decrease in particle size represents a clear strategy for raising E_{bound} while maintaining a high η, as shown for instance for the SBA-15 material. A special advantage of mesoporus silica materials is that fabricating them as small-sized particles is readily possible using established technology. Ability of advanced synthetic methods to also fine-tune the external morphology and the uniformity in

particle size of OMSM, as shown herein for the PSSP-type materials, provides additional opportunities for material design to enhance both the E_{bound} and the η for an optimum *Cat*.

CONCLUSIONS

Our study supports, and makes a strong case for, the integration of materials science and enzyme engineering in the development of high-performance enzyme immobilizates, and even co-immobilizates, on mesoporous silica for heterogeneous biocatalysis applications. Since the problems of low η dependent on E_{bound} is severe in particular for heterogeneously catalyzed biotransformation requiring molecular O_2 as the substrate, we expect that our considerations, while being relevant in general, will be of special importance to immobilized oxidase and oxygenase systems.[11,69,70]
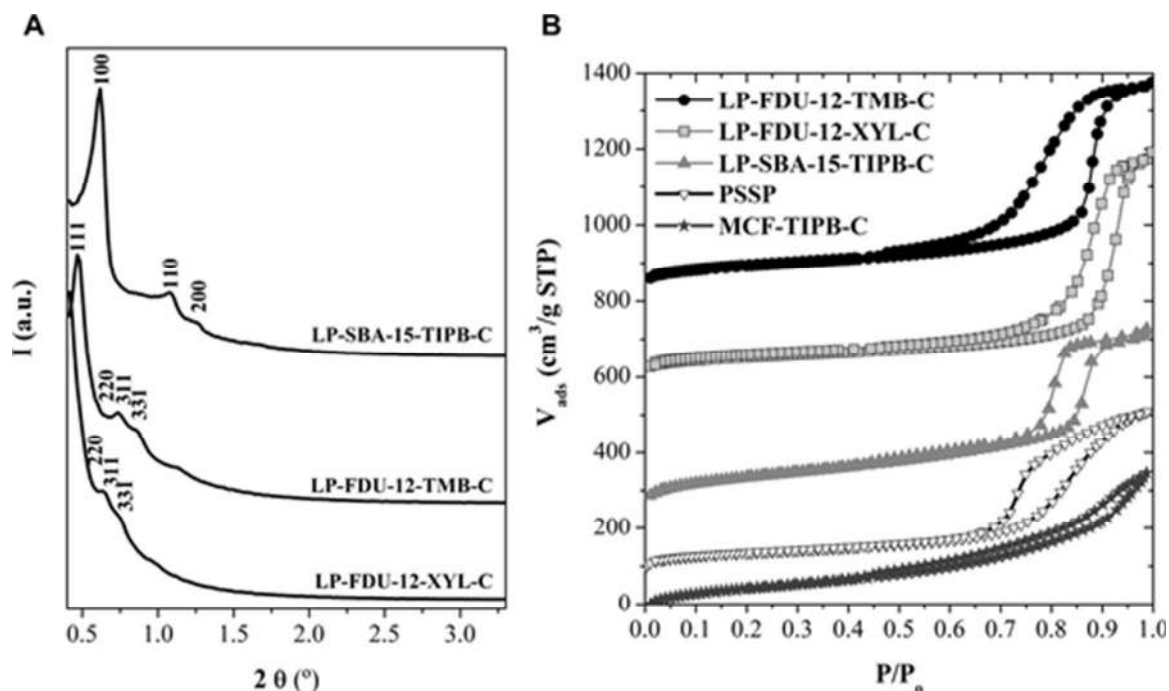
Figure 1. Structural characterization of silica materials is shown. Panel **A** shows the low-angle XRD diffractions. The patterns were overlaid and offset vertically to facilitate comparison from the top to the bottom of, respectively, LP-SBA-15-TIPB-C, LP-FDU-12-XYL-C and LP-FDU-12-TMB-C. The three materials gave the following reflections: 100, 110, 200 corresponding to a 2D hexagonal *p6mm* structure of the SBA-15 type material and 111, 220, 311 and 331 reflections, characteristic of a face-centered cubic structure (*Fm3m*), of the two FDU-12 type materials; all the XRD patterns are indicative of a very high degree of pore structural ordering. Panel **B** shows the nitrogen adsorption-desorption isotherms at -196 °C. The isotherms have been shifted vertically for clarity (LP-FDU-12-TMB-C +724 cm^3/g, LP-FDU-12-XYL-C +600 cm^3/g, LP-SBA-15-TIPB-C +225 cm^3/g and PSSP +75 cm^3/g, respectively). All materials exhibited typical type IV isotherms with adsorption-desorption hysteresis loops. The isotherm of LP-SBA-15-TIPB-C shows a type H1 hysteresis loop typical of a channel-like pore structure. The hysteresis loops of the isotherms corresponding to the others samples are of the H2b type, and are typical for materials with cage-like mesopores.
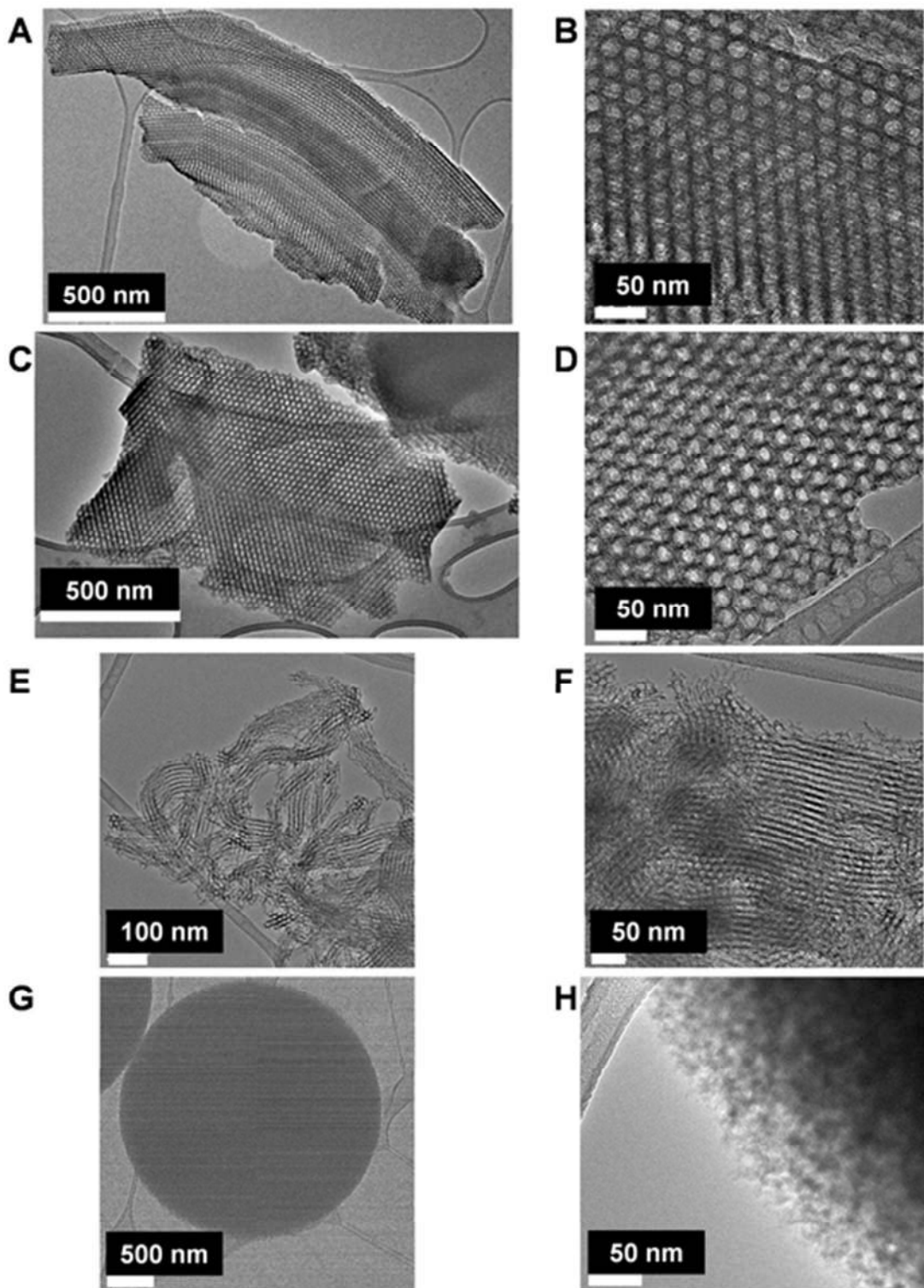
Figure 2. TEM images of calcined ordered mesoporous silica supports are shown. The panels show: LP-FDU-12-TMB-C (A, B), LP-FDU-12-XYL-C (C, D) and LP-SBA-15-TIPB-C (E, F) and amorphous silica PSSP (G, H). For more details, see *Methods section*.
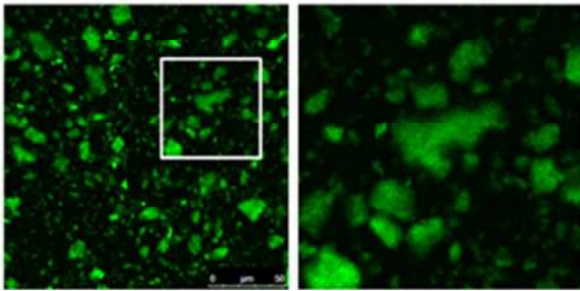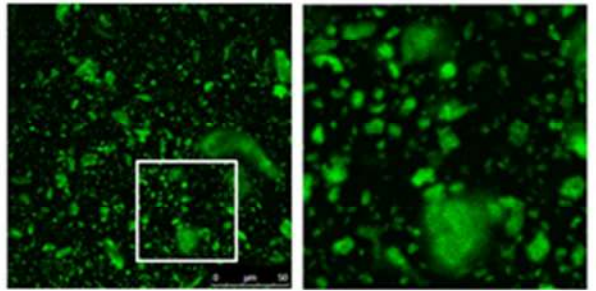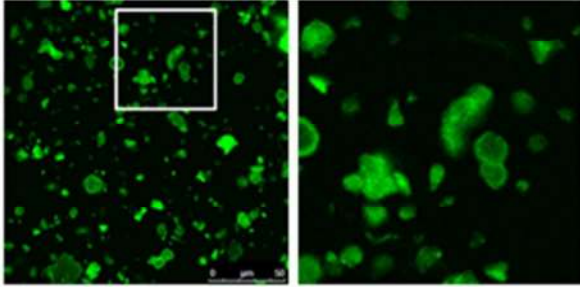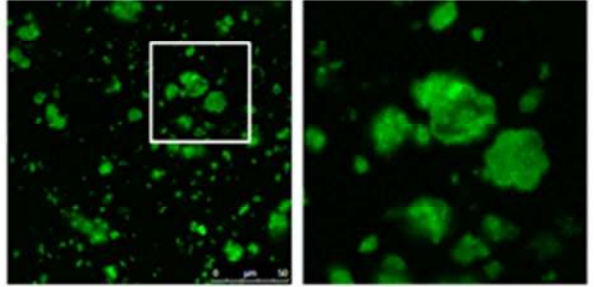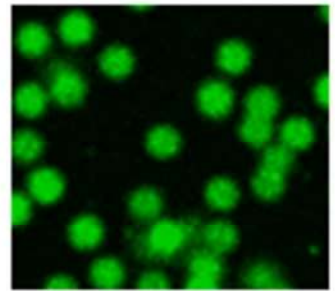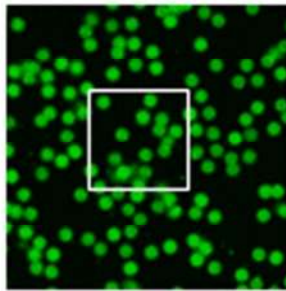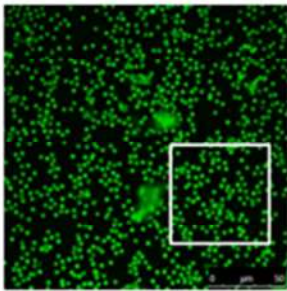
Figure 3. Confocal fluorescence images of Z_{basic2}_DAAO immobilized on silica supports are shown. Scale bars indicate 50 μm. The framed areas are shown with an additional 3-fold magnification.
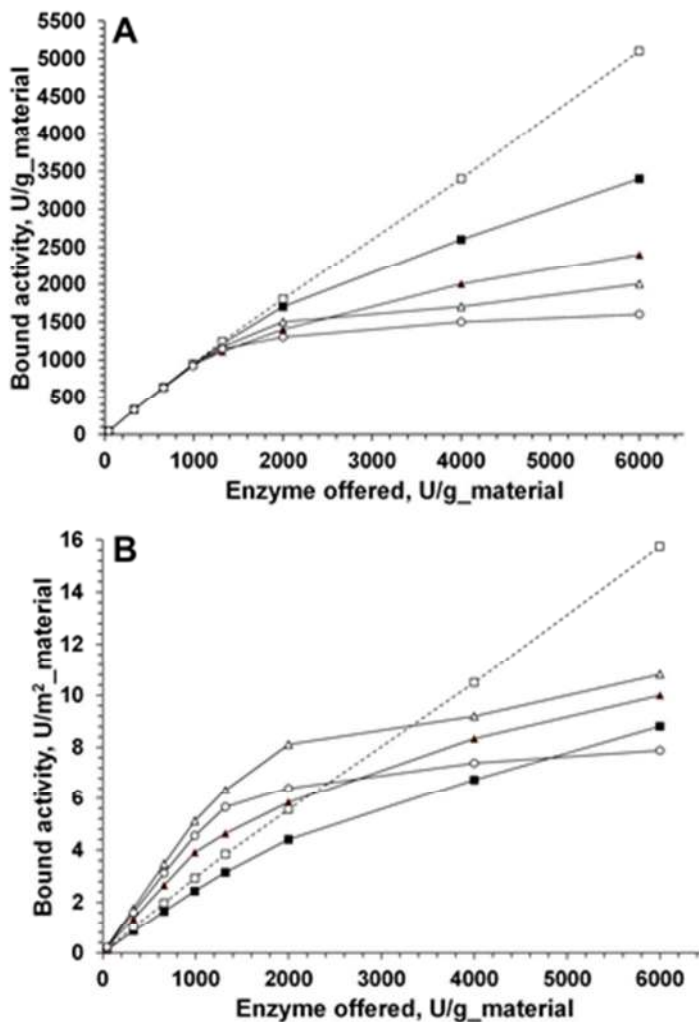
Figure 4. Immobilization of Z_{basic2}_DAAO on silica materials is shown. MCF-TIPB-C (solid squares), LP-SBA-15-TIPB-C (open squares), LP-FDU-12-TMB-C (solid triangles), LP-FDU-12-XYL-C (open triangles), PSSP (open circles) are shown. The bound activity, $E_{bound,}$ (Panel A) was calculated from the immobilization balance. E_{bound}/unit surface area of the materials (Panel B) was calculated using specific
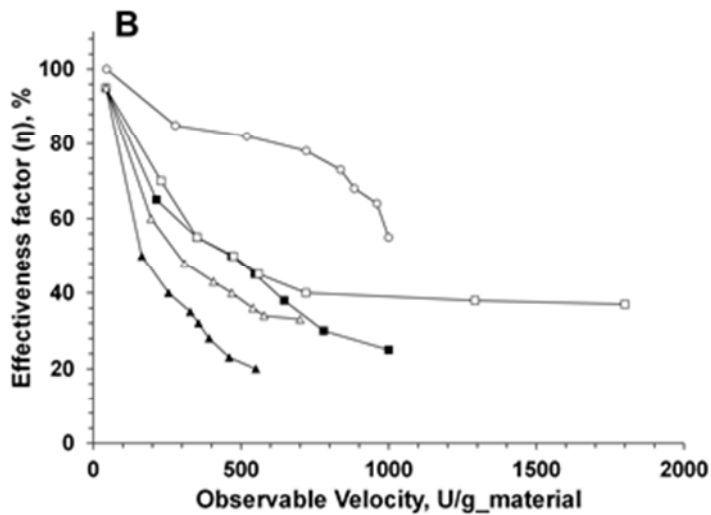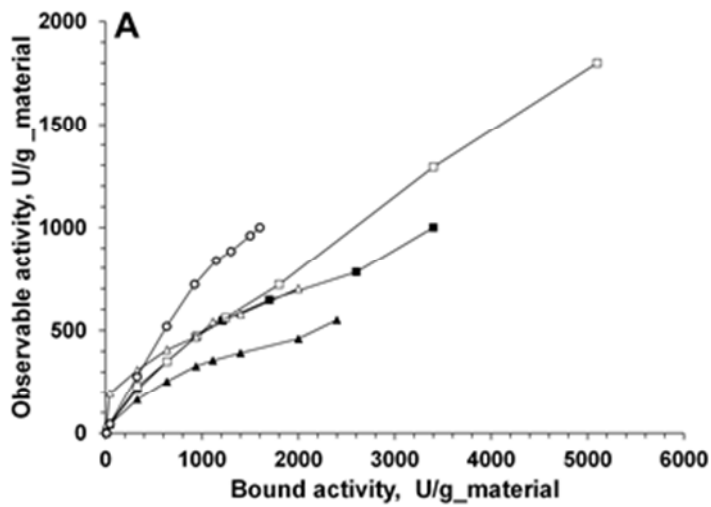
Figure 5. Observable activity E_{obs} (Panel A) and effectiveness factor η (Panel B) of Z_{basic2}_DAAO immobilizates in the oxidation of D-Met are shown. The symbols show Z_{basic2}_DAAO immobilized into MCF-TIPB-C (solid squares), Z_{basic2}_DAAO immobilized into LP-SBA-15-TIPB-C (open squares), Z_{basic2}_DAAO immobilized into LP-FDU-12-TMB-C (solid triangles), Z_{basic2}_DAAO immobilized into LP-FDU-12-XYL-C (open triangles) and Z_{basic2}_DAAO immobilized into PSSP (open circles). η is the ratio between E_{obs} and E_{bound}. Reactions were performed at 30 ºC using air-saturated potassium phosphate buffer (50 mM; pH 8.0). For more details, see the *Methods Section*.
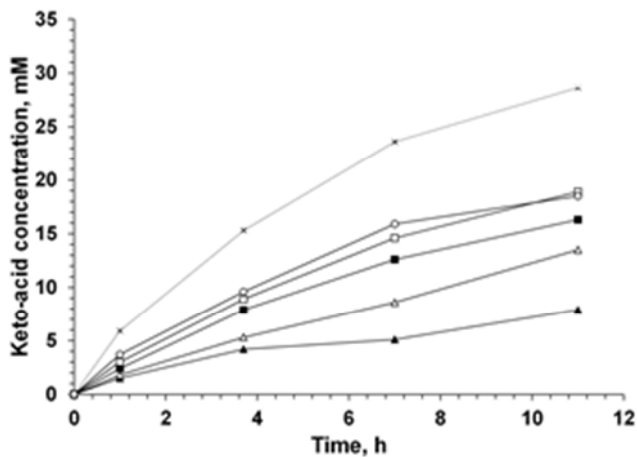
Figure 6. Batchwise oxidations of D-Met (50 mM) into 2-keto-4-(methylthio)butyric acid using soluble or silica-supported preparations of Z_{basic2}_DAAO and catalase at equivalent volumetric enzyme loading of 0.1 μmol/(min mL) are shown. The symbols show Z_{basic2}_DAAO immobilized into MCF-TIPB-C (solid squares), LP-SBA-15-TIPB-C (open squares), LP-FDU-12-TMB-C (solid triangles), LP-FDU-12-XYL-C (open triangles) and PSSP (open circles). For more details, see the *Methods Section*.

SCHEMES

Scheme 1. Suiting silica materials by design to the dimension of target proteins to be immobilized.
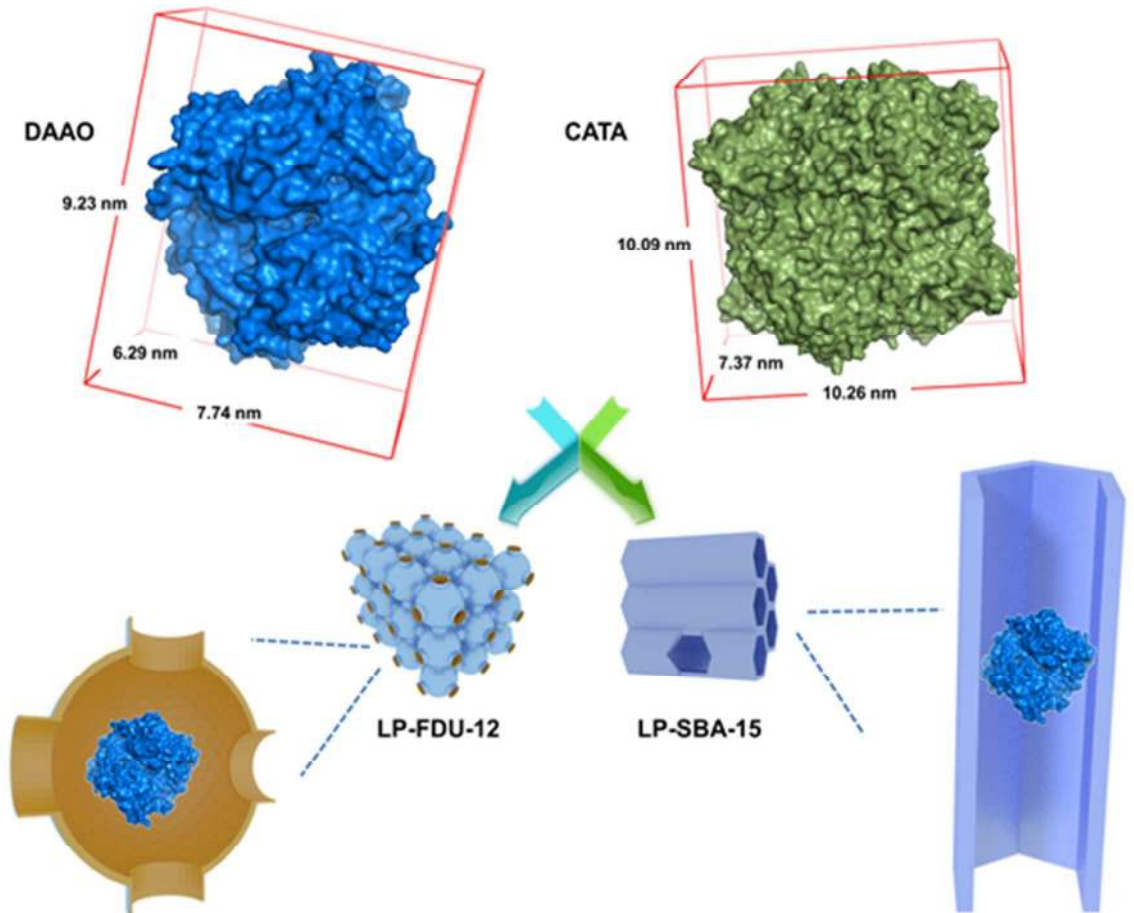
Scheme 2. The design window for the immobilization of an oxidase with the goal of optimizing the catalyst productivity, *Cat* (= $E_{bound} \eta$), is shown. Constraints on the design are indicated with dotted lines, revealing major limitations due to enzyme loading (Area I) and η (Area II). Boosting E_{bound} to enter Area IV requires material design. Boosting η to enter Area III requires identification and removal of the overall limiting factor, which could be immobilization chemistry or mass transport. Both could be addressed via material design as discussed in text. The current scenario of DAAO immobilized into mesoporous silica materials is displayed in the graph with diamonds and continuous line.
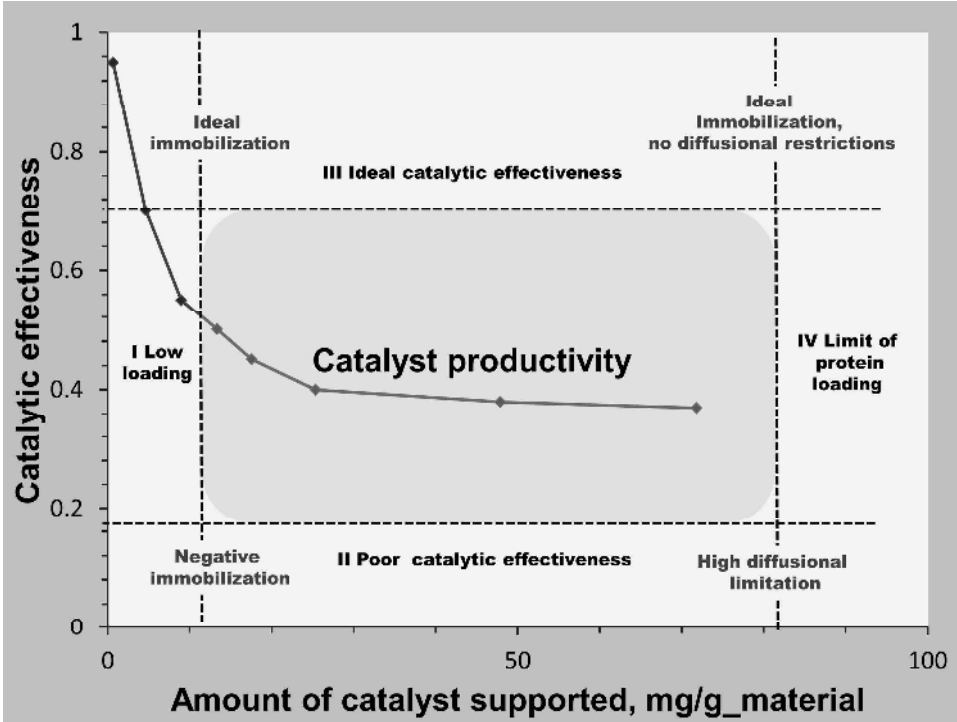
TABLES.

Table 1. Textural and structural parameters of the silica materials used are shown.

Material	Pore size (nm)[a]	Pore volume (cm^3/g)[b]	Surface area (m^2/g)[c]	a_o (nm)[d]
LP-FDU-12-TMB-C	9 [18]	0.9	240	40
LP-FDU-12-XYL-C	17 [31]	0.9	185	46
LP-SBA-15-TIPB-C	10	0.8	386	14
MCF-TIPB-C	5-30	0.6	324	-
PSSP	7 [12]	0.7	203	-

[a] Size of pore openings estimated from BJH pore size distribution (nitrogen isotherm desorption branch). Values between brackets indicate the estimated size of cages for structures with cage-type of pores.

[b] Pore volume (cm^3/g) estimated from the amount of nitrogen adsorbed at the relative pressure of 0.98.

[c] BET specific surface area (m^2/g).

[d] Unit cell parameter determined by XRD.

Table 2. The immobilization yield and the effectiveness factor of different co-immobilizates of

DAAO and CATA are shown.

Material	Immobilization yield[a]		Effectiveness factor, η, %[b]	
	CATA	DAAO	CATA	DAAO
LP-FDU-12-TMB-C	100	65	91	35
LP-FDU-12-XYL-C	100	70	75	45
LP-SBA-15-TIPB-C	100	85	47	65
MCF-TIPB-C	100	95	76	45
PSSP	100	95	98	80

[a] Immobilization of Z_{basic2}_DAAO and CATA on silica materials. Immobilization yield is the ratio of bound activity and initially offered. 2000 U of DAAO and 120000 U of catalase were offered per gram of solid material.

[b] Effectiveness factor, η, is the ratio between E_{obs} and E_{bound}. E_{bound} is calculated from the immobilization balance. For more details, see the *Methods Section*.

Table 3. The operational effectiveness factor (%) of different co-immobilizates of DAAO and CATA are shown.

Material	Effectiveness factor, η_{op}[a]		
	1st cycle	2nd cycle	3rd cycle
LP-FDU-12-TMB-C	30	25	15
LP-FDU-12-XYL-C	35	30	20
LP-SBA-15-TIPB-C	65	63	65
LP-SBA-15-TIPB-C*	45	< 5	0
MCF-TIPB-C	50	45	40
PSSP	65	50	40

[a] The operational effectiveness factor, η_{op}, was calculated as the ratio between initial oxidation rate given by heterogeneous biocatalysts and the oxidation rate given by 0.1 U/mL of free enzyme. All immobilizates contains 2000 U/g carrier of DAAO loading and 120000 U/g carrier of CATA loading. LP-SBA-15-TIPB-C* only contains DAAO. Heterogeneous biocatalyst were completely reused and used for new round of conversions. For more details, see the *Methods Section*.

ASSOCIATED CONTENT

Supporting Information. Preparation of silica supports; low-angle XRD patterns of amorphous mesoporous silica materials (Figure S1); SEM images of silica supports used (Figure S2 - S6); analysis of the pore size distributions of silica supports (Figure S7); transmission microscope images of silica supports (Figure S8); immobilization yield of the immobilization of Z_{basic2}_DAAO on the different silica supports (Figure S9); pore filling effect of immobilization of Z_{basic2}_DAAO on the different silica supports (Figure S10); time-scale analysis for diffusion and enzymatic reaction into Z_{basic2}_DAAO immobilizates (Figure S11). This material is available free of charge via the Internet at http://pubs.acs.org

AUTHOR INFORMATION

Corresponding Author

*Prof. Bernd Nidetzky, Institute of Biotechnology and Biochemical Engineering, Graz University of Technology, NAWI Graz, Petersgasse 12, A-8010 Graz, Austria; phone: +43 316 873 8400; fax: +43 316 873 8434; e-mail: bernd.nidetzky@tugraz.at

Author Contributions

All authors have given approval to the final version of the manuscript.

REFERENCES

(1) DiCosimo, R.; McAuliffe, J.; Poulose, A. J.; Bohlmann, G. Industrial Use of Immobilized Enzymes. *Chem. Soc. Rev.* **2013**, *42*, 6437-6474.

(2) Garcia-Galan, C.; Berenguer-Murcia, A.; Fernandez-Lafuente, R.; Rodrigues, R. C. Potential of Different Enzyme Immobilization Strategies to Improve Enzyme Performance. *Adv. Synth. Catal.* **2011**, *353*, 2885–2904.

(3) Franssen, M. C. R.; Steunenberg, P.; Scott, E. L.; Zuilhof, H.; Sanders, J. P. M. Immobilised Enzymes in Biorenewables Production. *Chem. Soc. Rev.* **2013**, *42*, 6491–6533.

(4) Liese, A.; Hilterhaus, L. Evaluation of Immobilized Enzymes for Industrial Applications. *Chem. Soc. Rev.* **2013**, *42*, 6236-6249

(5) Rodrigues, R. C.; Ortiz, C.; Berenguer-Murcia, Á.; Torres, R.; Fernández-Lafuente, R. Modifying Enzyme Activity and Selectivity by Immobilization. *Chem. Soc. Rev.* **2013**, *42*, 6290-6307.

(6) Hanefeld, U.; Gardossi, L.; Magner, E. Understanding Enzyme Immobilisation. *Chem. Soc. Rev.* **2009**, *38*, 453–468.

(7) Bolivar, J. M.; Eisl, I.; Nidetzky, B. Advanced Characterization of Immobilized Enzymes as Heterogeneous Biocatalysts. *Catal. Today* **2016**, *259*, 66–80.

(8) Cantone, S.; Ferrario, V.; Corici, L.; Ebert, C.; Fattor, D.; Spizzo, P.; Gardossi, L. Efficient Immobilisation of Industrial Biocatalysts: Criteria and Constraints for the Selection of Organic Polymeric Carriers and Immobilisation Methods. *Chem. Soc. Rev.* **2013**, *42*, 6262–6276.

(9) Fried, D. I.; Brieler, F. J.; Fröba, M. Designing Inorganic Porous Materials for Enzyme Adsorption and Applications in Biocatalysis. *ChemCatChem* **2013**, *5*, 862–884.

(10) Santos, J. C. S. dos; Barbosa, O.; Ortiz, C.; Berenguer-Murcia, A.; Rodrigues, R. C.; Fernandez-Lafuente, R. Importance of the Support Properties for Immobilization or Purification of Enzymes. *ChemCatChem* **2015**, *7*, 2413–2432.

(11) Turner, N. J. Enantioselective Oxidation of C-O and C-N Bonds Using Oxidases. *Chem. Rev.* **2011**, *111*, 4073–4087.

(12) Hernandez, K.; Berenguer-Murcia, A.; C. Rodrigues, R.; Fernandez-Lafuente, R. Hydrogen Peroxide in Biocatalysis. A Dangerous Liaison. *Curr. Org. Chem.* **2012**, *16*, 2652–2672.

(13) Bolivar, J. M.; Schelch, S.; Mayr, T.; Nidetzky, B. Dissecting Physical and Biochemical Factors of Catalytic Effectiveness in Immobilized D-Amino Acid Oxidase by Real-Time Sensing of O_2 Availability Inside Porous Carriers. *ChemCatChem* **2014**, *6*, 981–986.

(14) Bolivar, J. M.; Consolati, T.; Mayr, T.; Nidetzky, B. Shine a Light on Immobilized Enzymes: Real-Time Sensing in Solid Supported Biocatalysts. *Trends Biotechnol.* **2013**, *31*, 194–203.

(15) Bolivar, J. M.; Consolati, T.; Mayr, T.; Nidetzky, B. Quantitating Intraparticle O2 Gradients in Solid Supported Enzyme Immobilizates: Experimental Determination of Their Role in Limiting the Catalytic Effectiveness of Immobilized Glucose Oxidase. *Biotechnol. Bioeng.* **2013**, *110*, 2086–2095.

(16) Bolivar, J. M.; Schelch, S.; Mayr, T.; Nidetzky, B. Mesoporous Silica Materials Labeled for Optical Oxygen Sensing and Their Application to Development of a Silica-Supported Oxidoreductase Biocatalyst. *ACS Catal.* **2015**, *5*, 5984–5993.

(17) Sukyai, P.; Rezić, T.; Lorenz, C.; Mueangtoom, K.; Lorenz, W.; Haltrich, D.; Ludwig, R. Comparing Soluble and Co-Immobilized Catalysts for 2-Ketoaldose Production by Pyranose 2-Oxidase and Auxiliary Enzymes. *J. Biotechnol.* **2008**, *135*, 281–290.

(18) Sun, J.; Du, K.; Song, X.; Gao, Q.; Wu, H.; Ma, J.; Ji, P.; Feng, W. Specific Immobilization of d-Amino Acid Oxidase on Hematin-Functionalized Support Mimicking Multi-Enzyme Catalysis. *Green Chem.* **2015**, *17*, 4465–4472.

(19) Switala, J.; Loewen, P. C. Diversity of Properties among Catalases. *Arch. Biochem. Biophys.* **2002**, *401*, 145–154.

(20) Lončar, N.; Fraaije, M. W. Catalases as Biocatalysts in Technical Applications: Current State and Perspectives. *Appl. Microbiol. Biotechnol.* **2015**, *99*, 3351–3357.

(21) Grigoras, A. G. Catalase immobilization—A Review. *Biochem. Eng. J.* **2017**, *117*, 1–20.

(22) Magner, E. Immobilisation of Enzymes on Mesoporous Silicate Materials. *Chem. Soc. Rev.* **2013**, *42*, 6213–6222.

(23) Hartmann, M.; Kostrov, X. Immobilization of Enzymes on Porous Silicas − Benefits and Challenges. *Chem. Soc. Rev.* **2013**, *42*, 6277–6289.

(24) Bernal, C.; Illanes, A.; Wilson, L. Heterofunctional Hydrophilic–Hydrophobic Porous Silica as Support for Multipoint Covalent Immobilization of Lipases: Application to Lactulose Palmitate Synthesis. *Langmuir* **2014**, *30*, 3557–3566.

(25) Hudson, S.; Cooney, J.; Magner, E. Proteins in Mesoporous Silicates. *Angew. Chem. Int. Ed.* **2008**, *47*, 8582–8594.

(26) Lebeau, B.; Galarneau, A.; Linden, M. Introduction for 20 Years of Research on Ordered Mesoporous Materials. *Chem. Soc. Rev.* **2013**, *42*, 3661.

(27) Pitzalis, F.; Monduzzi, M.; Salis, A. A Bienzymatic Biocatalyst Constituted by Glucose Oxidase and Horseradish Peroxidase Immobilized on Ordered Mesoporous Silica. *Microporous Mesoporous Mater.* **2017**, *241*, 145–154.

(28) Gascón, V.; Díaz, I.; Márquez-Álvarez, C.; Blanco, R. M. Mesoporous Silicas with Tunable Morphology for the Immobilization of Laccase. *Mol. Basel Switz.* **2014**, *19*, 7057–7071.

(29) Gascón, V.; Márquez-Álvarez, C.; Blanco, R. M. Efficient Retention of Laccase by Non-Covalent Immobilization on Amino-Functionalized Ordered Mesoporous Silica. *Appl. Catal. Gen.* **2014**, *482*, 116–126.

(30) Zhou, Z.; Hartmann, M. Progress in Enzyme Immobilization in Ordered Mesoporous Materials and Related Applications. *Chem. Soc. Rev.* **2013**, *42*, 3894–3912.

(31) Zhao, D.; Huo, Q.; Feng, J.; Chmelka, B. F.; Stucky, G. D. Nonionic Triblock and Star Diblock Copolymer and Oligomeric Surfactant Syntheses of Highly Ordered, Hydrothermally Stable, Mesoporous Silica Structures. *J. Am. Chem. Soc.* **1998**, *120*, 6024–6036.

(32) Zhao, D. Triblock Copolymer Syntheses of Mesoporous Silica with Periodic 50 to 300 Angstrom Pores. *Science* **1998**, *279*, 548–552.

(33) Wan, Y.; Zhao, D. On the Controllable Soft-Templating Approach to Mesoporous Silicates. *Chem. Rev.* **2007**, *107*, 2821–2860.

(34) Yamada, T.; Zhou, H.; Asai, K.; Honma, I. Pore Size Controlled Mesoporous Silicate Powder Prepared by Triblock Copolymer Templates. *Mater. Lett.* **2002**, *56*, 93–96.

(35) Kosuge, K.; Sato, T.; Kikukawa, N.; Takemori, M. Morphological Control of Rod- and Fiberlike SBA-15 Type Mesoporous Silica Using Water-Soluble Sodium Silicate. *Chem. Mater.* **2004**, *16*, 899–905.

(36)   Jin, Z.; Wang, X.; Cui, X. Synthesis and Morphological Investigation of Ordered SBA-15-Type Mesoporous Silica with an Amphiphilic Triblock Copolymer Template under Various Conditions. *Colloids Surf. Physicochem. Eng. Asp*. **2008**, *316*, 27–36.

(37)   Schmidt-Winkel, P.; Lukens, W. W.; Zhao, D.; Yang, P.; Chmelka, B. F.; Stucky, G. D. Mesocellular Siliceous Foams with Uniformly Sized Cells and Windows. *J. Am. Chem. Soc*. **1999**, *12*, 254–255.

(38)   Schmidt-Winkel, P.; Glinka, C. J.; Stucky, G. D. Microemulsion Templates for Mesoporous Silica. *Langmuir* **2000**, *16*, 356–361.

(39)   Lettow, J. S.; Han, Y. J.; Schmidt-Winkel, P.; Yang, P.; Zhao, D.; Stucky, G. D.; Ying, J. Y. Hexagonal to Mesocellular Foam Phase Transition in Polymer-Templated Mesoporous Silicas. *Langmuir* **2000**, *16*, 8291–8295.

(40)   Sun, J.; Zhang, H.; Ma, D.; Chen, Y.; Bao, X.; Klein-Hoffmann, A.; Pfänder, N.; Su, D. S. Alkanes-Assisted Low Temperature Formation of Highly Ordered SBA-15 with Large Cylindrical Mesopores. *Chem. Commun*. **2005**, *42*, 5343-5345.

(41)   Zhang, H.; Sun, J.; Ma, D.; Bao, X.; Klein-Hoffmann, A.; Weinberg, G.; Su, D.; Schlögl, R. Unusual Mesoporous SBA-15 with Parallel Channels Running along the Short Axis. *J. Am. Chem. Soc*. 2004, *126*, 7440–7441.

(42)   Teixeira, C. V.; Amenitsch, H.; Linton, P.; Lindén, M.; Alfredsson, V. The Role Played by Salts in the Formation of SBA-15, an in Situ Small-Angle X-Ray Scattering/Diffraction Study. *Langmuir* **2011**, *27*, 7121–7131.

(43)   Fulvio, P. F.; Pikus, S.; Jaroniec, M. Tailoring Properties of SBA-15 Materials by Controlling Conditions of Hydrothermal Synthesis. *J. Mater. Chem*. **2005**, *15*, 5049-5053.

(44)   Barbosa, O.; Ortiz, C.; Berenguer-Murcia, Á.; Torres, R.; Rodrigues, R. C.; Fernandez-Lafuente, R. Strategies for the One-Step Immobilization–purification of Enzymes as Industrial Biocatalysts. *Biotechnol. Adv*. **2015**, *33*, 435–456.

(45)   Bolivar, J. M.; Nidetzky, B. Positively Charged Mini-Protein Zbasic2 as a Highly Efficient Silica Binding Module: Opportunities for Enzyme Immobilization on Unmodified Silica Supports. *Langmuir* **2012**, *28*, 10040–10049.

(46)   Ikeda, T.; Kuroda, A. Why Does the Silica-Binding protein "Si-Tag" bind Strongly to Silica Surfaces? Implications of Conformational Adaptation of the Intrinsically Disordered Polypeptide to Solid Surfaces. *Colloids Surf. B Biointerfaces* **2011**, *86*, 359–363.

(47)   Wiesbauer, J.; Bolivar, J. M.; Mueller, M.; Schiller, M.; Nidetzky, B. Oriented Immobilization of Enzymes Made Fit for Applied Biocatalysis: Non-Covalent Attachment to Anionic Supports Using Zbasic2 Module. *ChemCatChem* **2011**, *3*, 1299–1303.

(48)   Bolivar, J. M.; Schelch, S.; Pfeiffer, M.; Nidetzky, B. Intensifying the O2-Dependent Heterogeneous Biocatalysis: Superoxygenation of Solid Support from H2O2 by a Catalase Tailor-Made for Effective Immobilization. *J. Mol. Catal. B Enzym*. **2016**, *134*, 302–309.

(49)   Abdallah, N. H.; Schlumpberger, M.; Gaffney, D. A.; Hanrahan, J. P.; Tobin, J. M.; Magner, E. Comparison of Mesoporous Silicate Supports for the Immobilisation and Activity of Cytochrome c and Lipase. *J. Mol. Catal. B Enzym*. **2014**, *108*, 82–88.

(50)   Budi Hartono, S.; Qiao, S. Z.; Jack, K.; Ladewig, B. P.; Hao, Z.; Lu, G. Q. M. Improving Adsorbent Properties of Cage-like Ordered Amine Functionalized Mesoporous Silica with Very Large Pores for Bioadsorption. *Langmuir* **2009**, *25*, 6413–6424.

(51)   Huang, L.; Yan, X.; Kruk, M. Synthesis of Ultralarge-Pore FDU-12 Silica with Face-Centered Cubic Structure. *Langmuir* **2010**, *26*, 14871–14878.

(52) Cao, L.; Man, T.; Kruk, M. Synthesis of Ultra-Large-Pore SBA-15 Silica with Two-Dimensional Hexagonal Structure Using Triisopropylbenzene As Micelle Expander. *Chem. Mater*. **2009**, *21*, 1144–1153.

(53) Kruk, M. Access to Ultralarge-Pore Ordered Mesoporous Materials through Selection of Surfactant/Swelling-Agent Micellar Templates. *Acc. Chem. Res*. **2012**, *45*, 1678–1687.

(54) Fan, J.; Yu, C.; Gao, F.; Lei, J.; Tian, B.; Wang, L.; Luo, Q.; Tu, B.; Zhou, W.; Zhao, D. Cubic Mesoporous Silica with Large Controllable Entrance Sizes and Advanced Adsorption Properties. *Angew. Chem. Int. Ed*. **2003**, *42*, 3146–3150.

(55) Kruk, M.; Jaroniec, M.; Sayari, A. Application of Large Pore MCM-41 Molecular Sieves To Improve Pore Size Analysis Using Nitrogen Adsorption Measurements. *Langmuir* **1997**, *13*, 6267–6273.

(56) Bolivar, J. M.; Nidetzky, B. Oriented and Selective Enzyme Immobilization on Functionalized Silica Carrier Using the Cationic Binding Module Z basic2: Design of a Heterogeneous D-Amino Acid Oxidase Catalyst on Porous Glass. *Biotechnol. Bioeng*. **2012**, *109*, 1490–1498.

(57) Yuan, P.; Yang, J.; Zhang, H.; Song, H.; Huang, X.; Bao, X.; Zou, J.; Yu, C. New Insight into Ordered Cage-Type Mesostructures and Their Pore Size Determination by Electron Tomography. *Langmuir* **2015**, *31*, 2545–2553.

(58) Ersen, O.; Parmentier, J.; Solovyov, L. A.; Drillon, M.; Pham-Huu, C.; Werckmann, J.; Schultz, P. Direct Observation of Stacking Faults and Pore Connections in Ordered Cage-Type Mesoporous Silica FDU-12 by Electron Tomography. *J. Am. Chem. Soc*. **2008**, *130*, 16800–16806.

(59) Carlsson, N.; Gustafsson, H.; Thörn, C.; Olsson, L.; Holmberg, K.; Åkerman, B. Enzymes Immobilized in Mesoporous Silica: A Physical-Chemical Perspective. *Adv. Colloid Interface Sci*. **2014**, *205*, 339–360.

(60) Bolivar, J. M.; Schelch, S.; Mayr, T.; Nidetzky, B. Dissecting Physical and Biochemical Factors of Catalytic Effectiveness in Immobilized D-Amino Acid Oxidase by Real-Time Sensing of O2 Availability Inside Porous Carriers. *ChemCatChem* **2014**, *6*, 981–986.

(61) Fernández-Lafuente, R.; Rodriguez, V.; Guisán, J. M. The Coimmobilization of D-Amino Acid Oxidase and Catalase Enables the Quantitative Transformation of D-Amino Acids (D-Phenylalanine) into α-Keto Acids (Phenylpyruvic Acid). *Enzyme Microb. Technol*. **1998**, *23*, 28–33.

(62) Lopez-Gallego, F.; Batencor, L.; Hidalgo, A.; Mateo, C.; Fernandez-Lafuente, R.; Guisan, J. M. One-Pot Conversion of Cephalosporin C to 7-Aminocephalosporanic Acid in the Absence of Hydrogen Peroxide. *Adv. Synth. Catal*. **2005**, *347*, 1804–1810.

(63) Betancor, L.; Hidalgo, A.; Fernández-Lorente, G.; Mateo, C.; Rodríguez, V.; Fuentes, M.; López-Gallego, F.; Fernández-Lafuente, R.; Guisan, J. M. Use of Physicochemical Tools to Determine the Choice of Optimal Enzyme: Stabilization of D-Amino Acid Oxidase. *Biotechnol. Prog*. **2003**, *19*, 784–788.

(64) López-Gallego, F.; Betancor, L.; Hidalgo, A.; Alonso, N.; Fernandez-Lorente, G.; Guisan, J. M.; Fernandez-Lafuente, R. Preparation of a Robust Biocatalyst of D-Amino Acid Oxidase on Sepabeads Supports Using the Glutaraldehyde Crosslinking Method. *Enzyme Microb. Technol*. **2005**, *37*, 750–756.

(65) Rocha-Martin, J.; Velasco-Lozano, S.; Guisán, J. M.; López-Gallego, F. Oxidation of Phenolic Compounds Catalyzed by Immobilized Multi-Enzyme Systems with Integrated Hydrogen Peroxide Production. *Green Chem*. **2014**, *16*, 303–311.

(66)   Gascón, V.; Díaz, I.; Blanco, R. M.; Márquez-Álvarez, C. Hybrid Periodic Mesoporous Organosilica Designed to Improve the Properties of Immobilized Enzymes. *RSC Adv.* **2014**, *4*, 34356-34368.

(67)   Bayne, L.; Ulijn, R. V.; Halling, P. J. Effect of Pore Size on the Performance of Immobilised Enzymes. *Chem. Soc. Rev.* **2013**, *42*, 9000–9010.

(68)   Bolivar, J. M.; Hidalgo, A.; Sánchez-Ruiloba, L.; Berenguer, J.; Guisán, J. M.; López-Gallego, F. Modulation of the Distribution of Small Proteins within Porous Matrixes by Smart-Control of the Immobilization Rate. *J. Biotechnol.* **2011**, *155*, 412–420.

(69)   Hollmann, F.; Arends, I. W. C. E.; Buehler, K.; Schallmey, A.; Buhler, B. Enzyme-Mediated Oxidations for the Chemist. *Green Chem.* **2011**, 13, 226–265.

(70)   Monti, D.; Ottolina, G.; Carrea, G.; Riva, S. Redox Reactions Catalyzed by Isolated Enzymes. *Chem. Rev.* **2011**, *111*, 4111–4140.

Table of Contents Graphic